

Zinc Oxide Nanowire Lateral Field Emission Devices and its Application as Display Pixel Structures

Duo Li, Juncong She, Shaozeng Xu, and Shaozhi Deng

Abstract—The rational design and fabrication of zinc oxide (ZnO) nanowire (NW) lateral field electron emission device and the possible application as a display pixel structure are reported. In the device, the cathode and anode are ranked side-by-side on the same panel. The NW-clusters were controlled to locally grow on the edges of the electrodes with different tilted status, i.e., in angle range of $75^\circ \sim 110^\circ$, $0^\circ \sim 110^\circ$, and $0^\circ \sim 57^\circ$, respectively. The devices with NWs at different tilt-angle showed distinct field electron emission properties. The device with $0^\circ \sim 57^\circ$ tilted NWs possess the best performance, i.e., an emission current of $9.3 \mu\text{A}$ (current density: 6.22 A/cm^2) was obtained at a low cathode-anode ($50 \mu\text{m}$ in separation) bias of 477 V . Stable cathodoluminescence was observed from the indium titanate oxide anode, suggests a possibility for display application. Mechanisms responsible for the enhanced field electron emission and the related device physics are proposed. Significantly, the low temperature ($\sim 80^\circ\text{C}$) solution-phase growth of ZnO NWs enables the fabrication of the devices on flexible polyimide substrate, which has also been demonstrated here. This paper opens up possibilities on developing NW-based lateral field electron emission device for vacuum micro/nanoelectronics applications.

Index Terms—Electron trajectory, lateral field emission device, luminescence, nanowire (NW), pixel structure.

I. INTRODUCTION

FIELD electron emission display (FED) is a promising flat panel display technique owing to its superior characteristics of wide viewing angle, fast response time, and wide range of operating temperature [1]. So far, the FEDs were constructed in a configuration of a cathode panel assembled with an anode panel where accuracy alignments and massive microfabrication processes are

Manuscript received May 8, 2013; accepted July 3, 2013. This work was supported in part by the Projects from the National Basic Research Program of China under Grant 2010CB327703, the National Natural Science Foundation of China under Grant 51272293 and 61222111, the Science and Technology Department of Guangdong Province, the Economic and Information Industry Commission of Guangdong Province, the Science & Technology and Information Department of Guangzhou City, the projects from FANEDD under Grant 200927, the Program for New Century Excellent Talents in University under Grant NCET-10-0855, and the Doctoral Fund of Ministry of Education of China under Grant 20120171110018. The review of this paper was arranged by Editor M. Thumm.

The authors are with the State Key Laboratory of Optoelectronic Materials and Technologies, Guangdong Province Key Laboratory of Display Material and Technology, School of Physics and Engineering, Sun Yat-sen University, Guangzhou 510275, China (e-mail: shejc@mail.sysu.edu.cn).

Color versions of one or more of the figures in this paper are available online at <http://ieeexplore.ieee.org>.

Digital Object Identifier 10.1109/TED.2013.2272597

needed [1]–[4]. The development of the lateral field electron emission device may provide an alternative strategy for FED fabrication. In a lateral field electron emission device the integral anode and cathode are arrayed on the same substrate [5]–[10]. It may form a display pixel if the anode is covered with a luminescent material on the top-surface and the emitted electrons from the cathode can be drawn to bombard this surface to induce luminescence. This configuration has the advantages of self-aligned cathode-to-anode (one-mask-process), precise control of cathode-anode spacing, and easy integration of the gate electrodes [9]. However, the emitters fabricated by the traditional 2-D microfabrication processes are well parallel to the substrate surface [6]–[10]. In operation, the emitted electrons are drawn toward the sidewall of the anode, with less possibility to reach the anode top-surface. Recent developments on 1-D nanostructure cold cathode materials [11]–[13] provide a possibility on solving this problem, i.e., precisely control the nanoemitters to locally grow on the electrode sidewalls and make them incline to the substrate surface. Massive amount of electrons from the inclined emitters may reach the anode top-surface to induce a luminescence image. So far, the feasibility of this strategy has not been demonstrated yet.

In this paper, we report the fabrication, characterization, and the related device physics of the zinc oxide nanowire (ZnO NW) lateral field electron emission devices and its application as a display pixel structure. ZnO NW emitters were precisely controlled to grow on the electrode sidewalls using a low temperature ($\sim 80^\circ\text{C}$) solution-phase method [14]–[16]. The developed method has the advantages of low temperature growth, ease to scale up, and compatible to traditional semiconductor microfabrication process. It is rather essential for the low temperature process which makes it possible to fabricate devices on a glass or even on a flexible polymer substrate.

II. EXPERIMENT

The lateral field electron emission devices were fabricated on both glass and flexible polyimide (PI). The thickness, surface roughness (rms), and glass transition temperature of the PI substrate are $30 \mu\text{m}$, $\sim 3.4 \text{ nm}$ and $\sim 343^\circ\text{C}$, respectively. The PI sheet was mechanically rolled out on a glass carrier to keep a flat state for device microfabrication. A Si_3N_4 (100 nm) buffer layer was deposited on the PI surface by plasma enhanced chemical vapor deposition (Oxford Plasma Lab 80 plus) before the fabrication.

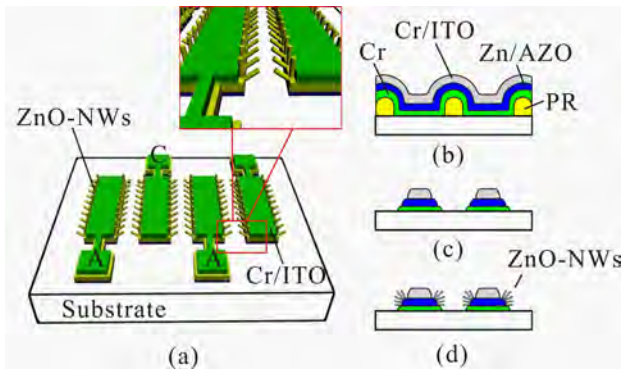


Fig. 1. (a) Schematic layout of the ZnO NW lateral field electron emission pixel structure. (b)–(d) Sketch for the fabrication procedure.

Fig. 1(a) shows the schematic layout of the ZnO NWs lateral field electron emission pixel structure. Electrode patterns with 500- μm length, 250- μm width, and 50- μm spacing are ranked side-by-side. They are severed as anode and cathode [shown as A and C in Fig. 1(a)], respectively. The ZnO nanoemitters grow on the sidewalls are sloped to the substrate surface. The patterns were fabricated by using a photoresist lift-off and the microfabrication procedure is shown in Fig. 1(b)–(d). In the fabrication, sputtered conductive films (i.e., Cr or ITO) and seed-layers [i.e., Zn or aluminum doped ZnO (AZO)] were deposited in sequence to form sandwich structures of Cr/Zn/ITO, Cr/Zn/Cr, Cr/AZO/ITO, and Cr/AZO/Cr for comparative studies. The seed-layers are used for inducing the growth of ZnO NWs [14]–[16]. The thickness of the Zn and AZO is 150 nm, while that for Cr and ITO is 200 nm. The bottom Cr layer was used to improve the adhesion between the seed-layer and the substrate. The growth of ZnO NWs was performed at 80 °C for 12 h in an aqueous solution of zinc nitrate hexahydrate ($\text{ZnO}(\text{NO}_3)_2 \cdot 6\text{H}_2\text{O}$) and hexamethylenetetramine [14]–[16]. The concentration of the aqueous solution was 1 mmol/L. The samples were put into the solution with the patterned side facing downward. After the growth, the samples were cleaned with deionized water, and dried by a nitrogen flow [Fig. 1(d)].

Scanning electron microscopy [(SEM), ZEISS SUPRA 55] and transmission electron microscope [(TEM), JEM-2010HR] were used to examine the morphology and structure of the ZnO NWs and the lateral field electron emission device. X-ray diffraction [(XRD), D-MAX 2200 VPC] with Cu $K\alpha$ radiation was employed to characterize the crystalline structure of the seed-layers. Atomic force microscopy [(AFM), Binnig CSPM 5500] was used to investigate the surface morphology of the Cr and ITO films. The field electron emission characteristics of the ZnO NWs lateral field electron emission device were investigated in a vacuum chamber with a base pressure of 2.0×10^{-5} Pa. The chamber with the samples in was baked at 140 °C for 24 h for degassing before performing the field emission tests. The field emission current was measured as a function of the applied voltage. The anode was biased by a power supply and the current was monitored by a picoampere meter (Keithley 6487).

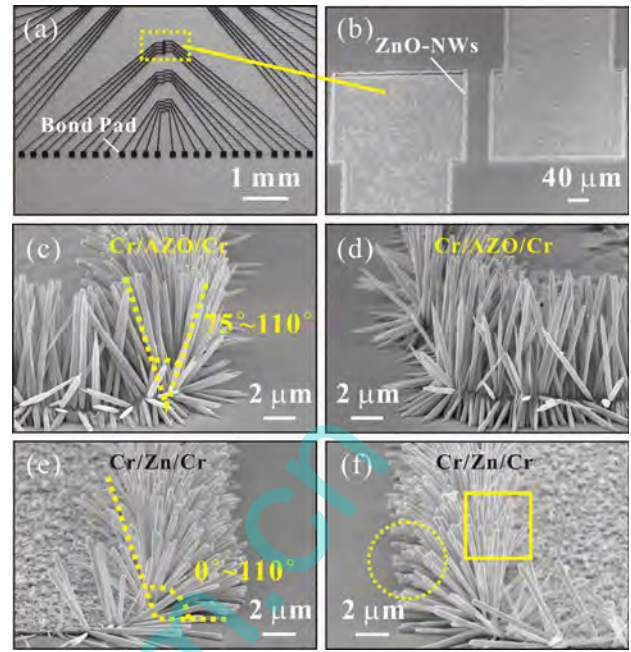


Fig. 2. (a) Typical optical microscopy and (b) low magnification SEM image of the ZnO NWs lateral field electron emission device fabricated on a glass substrate. (c)–(f) Typical SEM images (70° tilt-view) of the ZnO NWs with different sloping angles. Herein, (c)–(f) were taken from the devices with the Cr/AZO/Cr and Cr/Zn/Cr structures, respectively.

III. RESULTS AND DISCUSSION

A. Device on Glass Substrate

Fig. 2 shows the typical microscopy images of the lateral field electron emission device fabricated on a glass substrate. Electrode pairs with 500- μm length, 250- μm width, and 50- μm spacing are shown in Fig. 2(a) and (b). High magnification SEM investigations found that the seed-layer (Zn or AZO) has significant effect on the alignment of the ZnO NW. Fig. 2(c) and (d) are the typical SEM images (70° tilt-view) of the ZnO NWs grown on the left and right sidewalls of the Cr/AZO/Cr electrodes, respectively. They are arranged in a narrow tilt-angle range of 75° ~ 110°, with respect to the substrate surface. It is, however, clearly seen that the ZnO NWs grown on the sidewall of the Cr/Zn/Cr electrodes showing wider spread-out angles of 0° ~ 110° [Fig. 2(e) and (f)]. In both devices, the ZnO NWs are typically ~ 6.0 μm in height and ~ 320 nm in diameter. TEM investigation demonstrates that the ZnO NW is in well crystallization with growth direction of [0001] [14]–[16].

For interpreting the seed-layer effect on the alignment of the ZnO NW, Fig. 3(a) and (c) shows the typical SEM images of the Cr/AZO/Cr and Cr/Zn/Cr patterns. It is clear that both the edges of the AZO and Zn were exposed after lift-off. AFM analysis found that the typical surface roughness (rms) of the as-deposited AZO and Zn seed-layer are 2.99 and 15.60 nm [Fig. 3(e) and (f)], respectively. The rougher surface of the Zn film may improve the mechanical adhesion between the Zn and the top Cr layer. Therefore, less area of Zn film was exposed on the edge [Fig. 3(d)]. In the XRD spectrum of the AZO seed-layer [Fig. 3(b)]; one main diffraction peak between

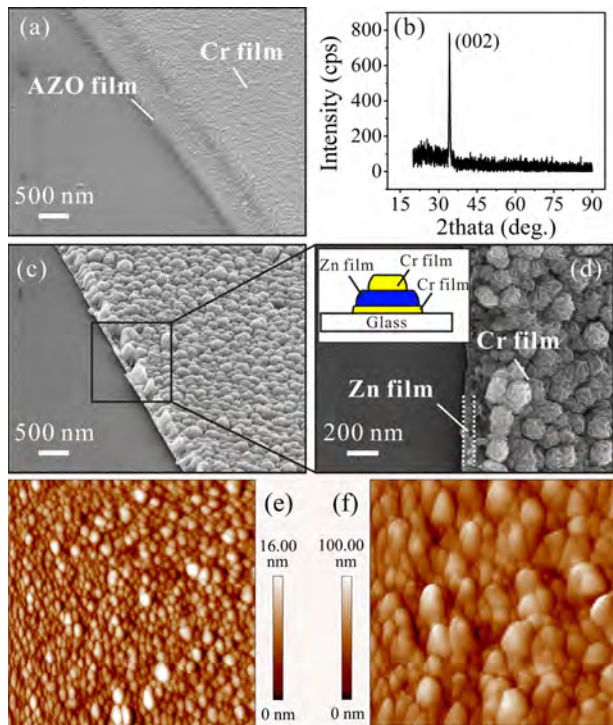


Fig. 3. (a) Typical SEM image showing the edge morphology of the Cr/AZO/Cr structure. (b) Typical XRD patterns of the AZO film. (c) and (d) Typical SEM image showing the edge morphology of the Cr/Zn/Cr structure. (e) and (f) Typical AFM images of the AZO and Zn films.

33° and 37° was identified. The peak is corresponding to the (002) lattice planes of the ZnO crystal. No main diffraction peak was, however, found in the XRD spectrum of Zn seed-layer. The XRD evidences suggest that the AZO film is much well crystallized than the Zn film. It is well accepted that (002) is the prior growth facet of ZnO crystal [14], [17]. Therefore, the NWs grown on the AZO surface are well aligned, i.e., with a tilt-angle range of $75^\circ \sim 110^\circ$ with respect to the substrate surface. The orientation of the NW grown on amorphous Zn is, however, relatively random, with larger spread-out angle of $0^\circ \sim 110^\circ$.

The field emission characteristics of the ZnO NWs lateral field electron emission device were investigated. The devices showed distinct field emission properties. No field emission was obtained from the devices with the NWs in tilt-angle range of $75^\circ \sim 110^\circ$ [Fig. 2(c) and (d)] before a breakdown event happened (typically at a 1 kV- cathode-anode bias). However, repeated current-voltage (I - V) characteristics (Fig. 4) were recorded from the device with $0^\circ \sim 110^\circ$ tilted NWs. Typically, an emission current of $0.22 \mu\text{A}$ was obtained at an anode-cathode bias of 430 V. The device can even operate at a high bias of 961 V with an emission current of $2.10 \mu\text{A}$. We took the sidewall area (roughly equal to the cathode area) for calculating the emission current density and a value of 1.40 A/cm^2 was obtained.

The Fowler-Nordheim (F-N) equation [18] is used to analyze the field emission behavior of the ZnO NWs. The F-N equation is given as

$$J = \left(\frac{a\beta^2 E^2}{\phi} \right) \exp \left(\frac{-B\phi^{3/2}}{\beta E} \right)$$

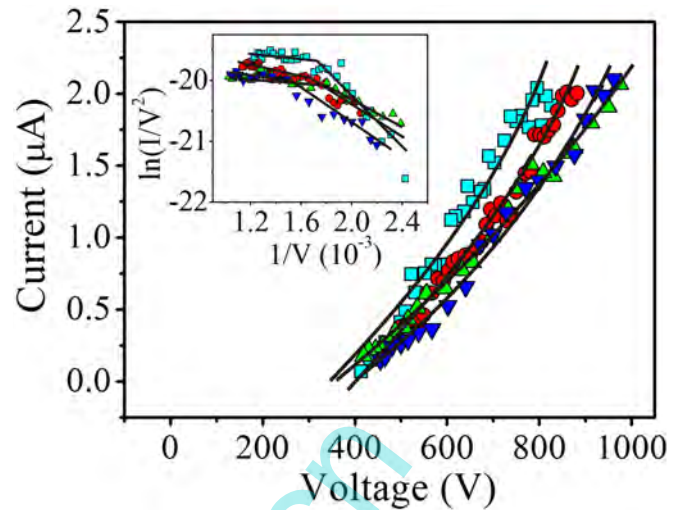


Fig. 4. Typical I - V curves and the corresponding F-N plots of the devices with $0^\circ \sim 110^\circ$ tilted NWs.

where J is the field emission current density ($\text{A} \cdot \text{m}^{-2}$), the constants $a = 1.56 \times 10^{-6} (\text{A} \cdot \text{eV} \cdot \text{V}^{-2})$, $B = 6.83 \times 10^9 (\text{V} \cdot \text{eV}^{-3/2} \cdot \text{m}^{-1})$, E is the apply field ($\text{V} \cdot \text{m}^{-1}$), β is the field enhancement factor, ϕ is the work function (eV). Furthermore, assuming that $J = I/S$ and $E = V/d$, where S is the emission area (m^2) and d is the separation between the anode and cathode (m^{-1}), we can obtain a linear relationship between $\ln(I/V^2)$ and $1/V$ as

$$\ln \left(\frac{I}{V^2} \right) = \ln \left(\frac{Sa\beta^2}{\phi d^2} \right) - \frac{Bd\phi^{3/2}}{\beta} \frac{1}{V}.$$

The inset of Fig. 4 shows the corresponding F-N plots of the devices with $0^\circ \sim 110^\circ$ tilted NWs. The F-N plots showing a clear nonlinearity and two distinct sections were observed. It is consistent well with the observation in one of our recent works [15]. We speculate that the current saturation in the high-voltage section is mainly due to the series resistance of the semiconductor ZnO NW and the seed-layers. In the lateral field electron emission device with a Cr/Zn/Cr structure [Fig. 2(e) and (f)], the ZnO NWs were locally grew on the electrode sidewalls and inclined to the substrate surface. It is distinct from other lateral field emission devices whose emitters are parallel to the substrate surface [6]–[10]. If the top Cr layer is replaced by a luminescent material and the emitted electrons from the cathode can be drawn to bombard the anode surface, the induced cathodoluminescence may form a display image. So far, the feasibility of this strategy has not been demonstrated yet. Herein, we replaced the top Cr film by an ITO layer. The use of the ITO film has two advantages. First, the deposition of the ITO film is well compatible to the device fabrication process. Second, the ITO has been widely used for displaying the field electron emission spatial distribution of the field emission cathodes [19], [20]. It may show clear luminescence image for the present purpose. Fig. 5(a) and (b) are the typical edge morphology of the Cr/Zn/ITO structure, showing a similar appearance to that of the Cr/Zn/Cr structure [Fig. 3(c) and (d)]. However, the ZnO NW growth on the sidewall of the Cr/Zn/ITO structure [Fig. 5(c) and (d)] shows

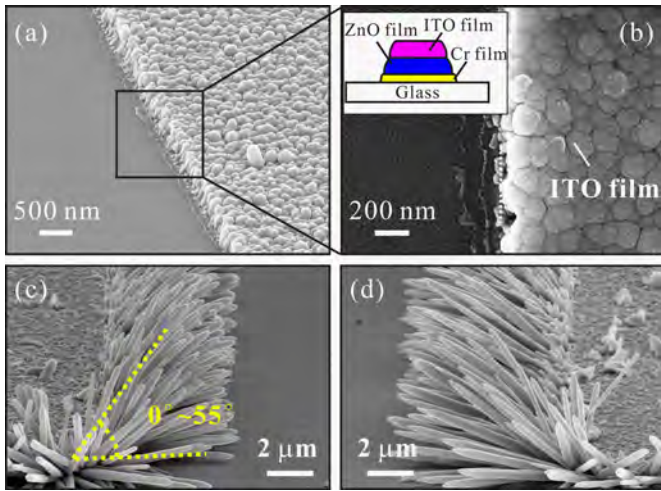


Fig. 5. (a) and (b) Typical SEM images showing the edge morphology of the Cr/Zn/ITO structure. (c) and (d) Typical SEM images (70° tilt-view) of the ZnO NWs grew on the sidewalls of the Cr/Zn/ITO structure with a spread-out angel range of $0^\circ \sim 57^\circ$.

a narrower spread-out angel range ($0^\circ \sim 57^\circ$) than that of the Cr/Zn/Cr structure [Fig. 3(c) and (d)]. The result suggests that less Zn seed-layer was exposed from the top ITO film in the lift-off. The magnetron sputtering deposition rate of the semiconductor ITO (5 nm/min) is much lower than that of the metallic Cr film (23 nm/min). The ITO film is much denser than that of the Cr film. It is reasonable to propose that the denser ITO film resulted in a less exposure of the underneath seed-layer in the lift-off. This qualitatively explains the difference in the NW alignment of the Cr/Zn/Cr and the Cr/Zn/ITO device structure.

The device with $0^\circ \sim 57^\circ$ tilted NWs possesses a better field electron performance than that of the device with $0^\circ \sim 110^\circ$ tilted NWs, i.e., much lower bias is needed to obtain the same emission current. Fig. 6(a) shows the typical I - V curves and the corresponding F-N plots. Typically, an emission current of $0.1 \mu\text{A}$ was obtained at an anode bias of 135 V with 50- μm anode-cathode spacing. The device can even operate at a high bias of 477 V with emission current of $9.33 \mu\text{A}$ (current density: 6.22 A/cm^2). More interestingly, during the measurement, one can observe stable bright spot from the device at the relatively high anode voltages. Fig. 6(b)–(d) shows the typical images of the bright spots at the anode biases of 450, 463, and 477 V with the corresponding emission currents of 7.43, 7.89, and $9.33 \mu\text{A}$, respectively. The size of the bright spot were enlarged with the increase of the applied voltage (accompany with a current increase). The highest brightness is rather weak ($\sim 3.0 \text{ cd/m}^2$). It may be due to the poor luminescence properties of the ITO anode and the low electron energy (accelerated voltage $\sim 477 \text{ V}$). The spot is in rectangle shape, respectively, $\sim 100 \mu\text{m}$ (at 450 V), $\sim 215 \mu\text{m}$ (at 463 V) and $\sim 250 \mu\text{m}$ (at 477 V) in width and $\sim 500 \mu\text{m}$ in length. The rectangle shape of the lighting pattern is consistent well with that of the electrode. Fig. 6(e)–(g) shows the typical SEM images of the ITO anode after the field emission test. It was found that the ITO anode surface is much rougher after the test. This may

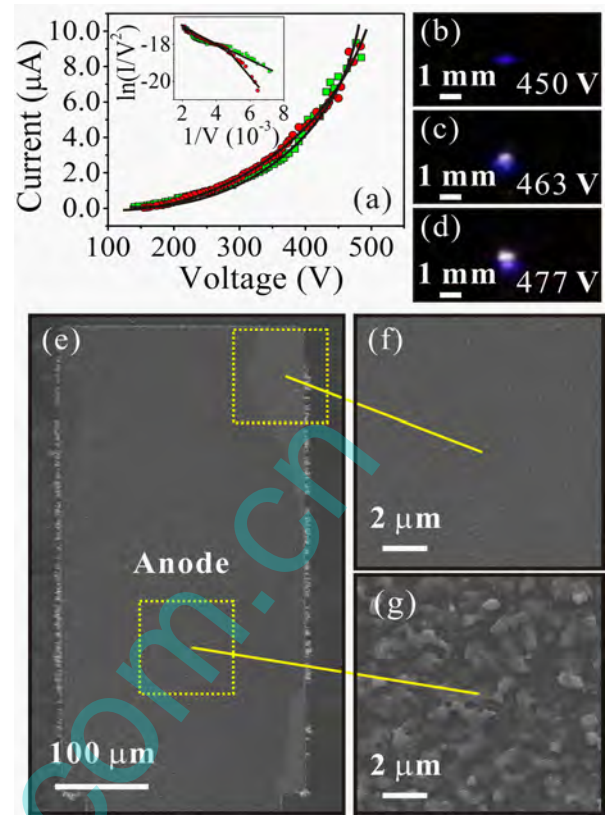


Fig. 6. (a) Typical I - V curves and F-N plots of the device with $0^\circ \sim 57^\circ$ tilted NWs. (b)–(d) Typical image of the bright spot observed at currents and voltages of (b) $7.43 \mu\text{A}$ at 450 V, (c) $7.89 \mu\text{A}$ at 463 V and (d) $9.33 \mu\text{A}$ at 477 V. (e)–(g) Typical SEM images of the anode surface after the field emission test.

due to the bombardment of the accelerated electrons. The far corner [Fig. 6(f)] of the ITO anode-electrode is smoother than those of the near corner and the center [Fig. 6(g)]. The clue suggests that the electrons may not reach the far corner of the ITO anode electrode. It is clear to see that the rougher surface covers almost the whole anode area, i.e., 250 μm in width and 500 μm in length, which is consistent well with the bright spot area [Fig. 6(d)]. The observation of the lighting spots from the ZnO NW lateral field electron emission device is an inspiration for developing lateral field emission device into FED application. However, challenges come out to make a practicable FED, i.e., how to: 1) improve the brightness using the novel low voltage phosphor materials; 2) realize the addressable arrays; and 3) achieve an encapsulation FED. Further research works are needed.

Although the possibility of the ZnO NW lateral field electron emission device for display pixel application was demonstrated, the understanding of the distinct field emission performance of the devices with different aligned NW needs further concerns. Thus, numerical simulations were performed. Fig. 7(a) shows the schematic layout of the 2-D simulation model of the device. The simulation was performed by employing commercial software of COMSOL multiphysics (Ver. 4.2). In the simulation, a NW was set as a metallic cylindrical shape with a diameter and a length of 1 and 10

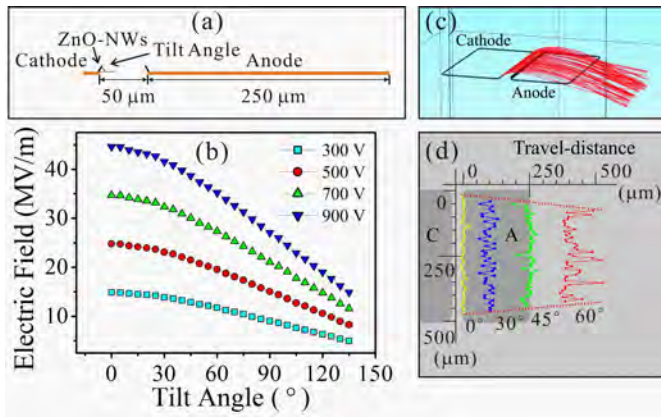


Fig. 7. (a) Schematic layout of a 2-D simulation model of the device. (b) Simulation results of the local electric field at the apex of the NWs under different anode bias. (c) Simulation result of the electron trajectories from NWs with 45° tilt-angle at a bias of 500 V. (d) Represented curves showing the electron landed positions at bias of 500 V. Inset values: tilt-angle of the NWs.

μm , respectively, for diminishing the computation scale and reducing the ratio of maximum to minimum model dimension. Electrodes with 250- μm width and 50- μm spacing were set. The cathode-anode bias is given in a range of 300~900 V with an increase interval of 200 V, while the tilt-angle of the NW is set as a serial of angle fallen in $0^\circ \sim 135^\circ$, with a 5° interval. Fig. 7(b) shows the typical simulation result. As shown in Fig. 7(b), following the enlarging of the tilt-angle, the local electric field at the apex of the NWs is linearly decreased. Typically, at a 500 V bias, the highest and the lowest electric fields are 24.79 and 15.05 MV/m for the emitters parallel and perpendicular to the substrate surface, respectively.

Although the simulation based on a predigested model (single emitter) cannot give the real electric field values, the findings on the relationship between the tilt-angle and the electric field gives a clear clue for understanding the experimental observations. According to the simulation results, NWs with a larger tilt-angle possesses a weaker local electric field (i.e., ineffective emitters). This corresponds well with our observation that no field emission was obtained from the devices with $75^\circ \sim 110^\circ$ tilted NWs [Fig. 2(c) and (d)]. On the contrast, devices with $0^\circ \sim 110^\circ$ [Fig. 2(e) and (f)] and $0^\circ \sim 57^\circ$ [Fig. 5(c) and (d)] tilted NWs both contain NW with lower tilt-angle and thus higher local electric field (i.e., effective emitters), which allows them to emit electrons at a relatively low anode voltage. We further compared the field screening effect of the $0^\circ \sim 110^\circ$ and $0^\circ \sim 57^\circ$ tilted NWs. For a single emitter, the field enhancement factor can be described as $\beta_{\text{single}} \propto h/r$, where h is the height and r is the radius of the emitter. However, for a NW array, the close spacing is a significant factor which brings field screening. A simple electrostatic model was proposed in [21] to estimate the field screening effect of the carbon nanotube (CNT) emitters. In the model, a screening factor was defined as $f(l) = \beta_{\text{array}}/\beta_{\text{single}}$. The $f(l)$ value varies from 0 to 1, where l is the separation between two adjacent emitters. Smaller $f(l)$ value means stronger field screening. Typically, for the emitters with height of $h_0 = 2 \mu\text{m}$, the $f(l)$ can be calculated

from a function of $f(l) = 1 - \exp(-1.1586l)$. To determine $f(l)$ for $h \neq h_0$, l was scaled by a factor of h_0/h , i.e., $f(l) = [1 - \exp(-1.1586l(h_0/h))]$ [21]. It is clear that the l/h ratio is the main factor for the screening effect. We compared the l and h values of the ZnO NW showing in Figs. 2(e) and 5(c). Although the NW in Fig. 5(c) shows a sharpen profile, no obvious different has been found for the l and h . However, it is clear shown in Fig. 2(f), the effective emitters (dot line circled) with smaller tilt-angle may be screened by the ineffective emitters (solid line circled) which have larger tilt-angle. This can qualitatively explain why the devices with $0^\circ \sim 57^\circ$ [Fig. 5(c) and (d)] tilted NWs possesses superior field emission performance than that with $0^\circ \sim 110^\circ$ tilted NWs [Fig. 2(e) and (f)].

We further used the same software to perform a 3-D numerical simulation for investigating the electron trajectory of the devices. The geometrical parameters employed for the simulation are the same as those of the actual device [Fig. 5(c) and (d)]. The initial velocity of the emitted electron was set as zero in magnitude and with a random direction. The anode voltage is fixed on 500 V. Here, a travel-distance [the values shown on the horizontal abscissa in Fig. 7(d)] is defined to describe the electron landed position on the anode surface. It was found that the tilt-angle has significant effect on the electron travel-distance. As shown in Fig. 7(d), at a certain cathode-anode bias (i.e., 500 V), larger tilt-angle will result in farther electron travel-distance. The emitted electrons from the NWs with $0^\circ - 45^\circ$ tilt-angle are all drew toward the anode surface. More interestingly, it was found that the electrons are concentrated follows the increase of the tilt-angle (red dot line indicated). Larger tilt-angle will result in a narrower distribution of the landed position. It is consistent well with the experimental observation shown in Fig. 6(e)–(g), i.e., the far corner of the ITO electrode is free from the electron bombardment.

We take the 2-D and 3-D numerical simulation results into the interpretation of the experimental observations on the display pixel structure. In Fig. 5(c) and (d), the NWs are spread-out in an angle-range of $0^\circ \sim 57^\circ$. The NWs with smaller tilt-angle have a higher local electric field on the apex. They emit electrons at a relatively low anode voltage (i.e., 450 V). Thus, a small rectangle bright spot was observed [Fig. 6(b)]. With the increase of the anode voltage, more emitters with larger tilt-angle were activated. Consequently, a larger bright spot was obtained [Fig. 6(d)]. Electrons from the $0^\circ \sim 57^\circ$ tilted NWs would cover most of the surface area of the anode, except the far corner.

B. Device on Flexible PI Substrate

Flexible FEDs have recently attracted intensive concern due to its unique portable and bendable features, which are considered appliances of great potential for flexible FEDs [22]–[24]. Already, flexible FEDs (diode structure) based on CNT [22], tungsten oxide NW [23], and graphene [24] have been reported. However, research has yet to be performed on fabricating lateral field electron emission devices on flexible substrate. Herein, the fabrica-

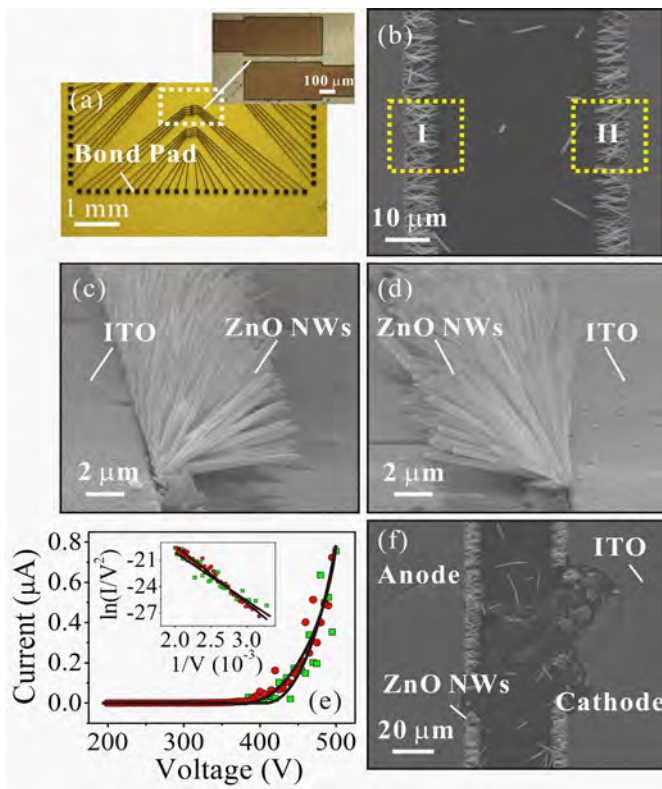


Fig. 8. (a) Typical optical microscopy image of the device fabricated on PI substrate. (b) top-view SEM image of the device. (c) and (d) Corresponding tilt-view (70°) SEM images of ZnO NWs in area I and II indicated in (b), respectively. (e) Typical field emission I - V and F - N plots of the devices on the PI substrate. (f) Typical SEM image of the device after undergoing a breakdown event.

tion and characterization of ZnO NW lateral field electron emission device on a flexible PI substrate were realized. The preparation and properties of the flexible PI substrate were described in the experiments section. Then, the devices were fabricated follow the same procedures shown in Fig. 1(b)-(d). Fig. 8(a)-(d) shows the typical optical microscopy and SEM images of the devices. The morphology of the NWs is similar to that shown in Fig. 5(c) and (d), suggested that the fabrication process is compatible to the flexible PI substrate. The field emission testing on the devices was also performed in the high vacuum chamber. Similar conditioning processes were carried out. During the baking, no obvious degas phenomenon was observed. Fig. 8(e) shows the typical I - V and F - N characteristics of the flexible devices. An emission current of 1.0 nA was obtained at an anode voltage of 350 V. A relatively high current of 1.0 μ A was obtained at an anode voltage of 495 V (current density: 0.67 A/cm²). It was found that a breakdown event would happen if the cathode-anode bias is increased up to 500 V [Fig. 8(f)]. It may due to the relatively weak insulation of the substrate surface. It is noted that the field emission performance of the flexible device is poorer than that of the device on glass, i.e., lower current density at the same applied anode voltage. No display pixel image was observed. More works are needed to clarify the discrepancy.

IV. CONCLUSION

We have reported a general method to fabricate a lateral field electron emission device using ZnO NWs with different tilt angles. The ZnO NW lateral field electron emission device can form a display pixel structure with stable luminescence image which is potentially for FED application. The low temperature hydrothermal growth of ZnO NW enables the fabrication of the devices even on flexible PI substrate. This paper provides a rational procedure for lateral field electron emission device fabrication. The low temperature process makes it possible to integrate the field electron emission device with traditional semiconductor device and enable us to promote the applications.

REFERENCES

- [1] A. A. Talin, K. A. Dean, and J. E. Jaskie, "Field emission display: A critical review," *Solid-State Electron.*, vol. 45, no. 6, pp. 963-976, 2001.
- [2] K. Qu, C. Li, K. Hou, X. X. Yang, J. Zhang, W. Lei, X. B. Zhang, B. P. Wang, and X. W. Sun, "High efficiency surface-conducted field emission from a ZnO nanotetrapod and MgO nanoparticle composite emitter," *Appl. Phys. Lett.*, vol. 93, no. 25, pp. 253501-1-253501-3, 2008.
- [3] J. Luo, J. Chen, S. Z. Deng, Y. Zhang, and N. S. Xu, "Double-gate-driving field emission display panel with stacked-metalized-aperture structure," *J. Vacuum Sci. Technol. B*, vol. 28, no. 2, pp. C2D15-C2D21, 2010.
- [4] H. J. Jeong, H. D. Jeong, H. Y. Kim, J. S. Kim, S. Y. Jeong, J. T. Han, D. S. Bang, and G. W. Lee, "All-carbon nanotube-based flexible field-emission devices: From cathode to anode," *Adv. Funct. Mater.*, vol. 21, no. 8, pp. 1526-1532, 2011.
- [5] H. H. Busta, J. E. Pogemiller, and M. F. Roth, "Lateral miniaturized vacuum devices," in *IEDM Tech. Dig.*, vol. 89, 1989, pp. 553-556.
- [6] Y. L. Liou, J. C. Liou, J. H. Huang, N. H. Tai, and I. N. Lin, "Fabrication and field emission properties of ultra-nanocrystalline diamond lateral emitters," *Diamond Rel. Mater.*, vol. 17, nos. 4-5, pp. 776-781, 2008.
- [7] N. S. Liu, G. J. Fang, W. Zeng, H. Long, X. Fan, L. Y. Yuan, X. Zou, Y. P. Liu, and X. Z. Zhao, "Strong effect of interelectrode distance on the performance of a novel ZnO nanorod lateral field emission device fabricated by a single-step hydrothermal approach," *J. Phys. Chem. C*, vol. 114, no. 18, pp. 8575-8580, 2010.
- [8] K. Subramanian, W. P. Kang, J. L. Davidson, B. K. Choi, and M. Howell, "Nanodiamond lateral comb array field emission diode for high current applications," *Diamond Rel. Mater.*, vol. 15, nos. 11-12, pp. 1994-1997, 2006.
- [9] K. Subramanian, W. P. Kang, J. L. Davidson, and M. Howell, "Nanodiamond lateral field emitter devices on thick insulator substrates for reliable high power applications," *Diamond Rel. Mater.*, vol. 17, nos. 4-5, pp. 786-789, 2008.
- [10] X. C. LeQuan, B. K. Choi, W. P. Kang, and J. L. Davidson, "Nanodiamond lateral device field emission diode fabricated by electron beam lithography," *Diamond Rel. Mater.*, vol. 19, nos. 2-3, pp. 252-255, 2010.
- [11] N. S. Xu and S. E. Huq, "Novel cold cathode materials and applications," *Mater. Sci. Eng. R.*, vol. 48, nos. 2-5, pp. 47-189, 2005.
- [12] J. B. Chen, C. J. Xu, J. C. She, S. Z. Deng, J. Chen, and N. S. Xu, "Pulsed-laser treatment of solution-grown ZnO nanowires in nitrogen: Enhancing in electrical conduction and field emission," *Appl. Phys. Lett.*, vol. 107, no. 2, pp. 024312-1-024312-3, 2010.
- [13] F. Liu, F. Y. Mo, S. Y. Jin, L. Li, Z. S. Chen, R. Sun, J. Chen, S. Z. Deng, and N. S. Xu, "A novel lift-off method for fabricating patterned and vertically-aligned W₁₈O₄₉ nanowire arrays with good field emission performance," *Nanoscale*, vol. 3, no. 4, pp. 1850-1854, 2011.
- [14] J. Liu, J. C. She, S. Z. Deng, J. Chen, and N. S. Xu, "Ultrathin seed-layer for tuning density of ZnO nanowire arrays and their field emission characteristics," *J. Phys. Chem. C*, vol. 112, no. 31, pp. 11685-11690, 2008.
- [15] W. J. Yang, J. C. She, S. Z. Deng, and N. S. Xu, "Field emission from a MOSFET-controlled ZnO nanowire cold cathode," *IEEE Trans. Electron Devices*, vol. 59, no. 12, pp. 3641-3646, Dec. 2012.
- [16] H. He, J. C. She, Y. F. Huang, S. Z. Deng, and N. S. Xu, "Precisely-controlled fabrication of single ZnO nanoemitter arrays and their possible application in low energy parallel electron beam exposure," *Nanoscale*, vol. 4, no. 6, pp. 2101-2108, 2012.

- [17] L. W. Feng, J. Liu, J. C. She, N. S. Xu, S. Z. Deng, and J. Chen, "Three-dimensional six-fold symmetry ZnO sub-microstructures," *J. Cryst. Growth*, vol. 311, no. 5, pp. 1435–1440, 2009.
- [18] R. H. Fowler and L. Nordheim, "Electron emission in intense electric fields," *Proc. R. Soc. London A, Math. Phys. Character.*, vol. 173, no. 781, pp. 173–181, 1928.
- [19] N. S. Xu, Y. Tzeng, and R. V. Latham, "Similarities in the 'cold' electron emission characteristics of diamond coated molybdenum electrodes and polished bulk graphite surfaces," *J. Phys. D, Appl. phys.*, vol. 26, no. 10, pp. 1776–1780, 1993.
- [20] H. Kiyota, H. Araki, H. Kobayashi, T. Shiga, K. Kitaguchi, M. Iida, H. Wang, T. Miyo, T. Takida, T. Kurosu, K. Inoue, I. Saito, M. Nishitani-Gamo, I. Sakaguchi, and T. Ando, "Electron field emission from diamond-like carbon films deposited by electrolysis of methanol liquid," *Appl. Phys. Lett.*, vol. 75, no. 15, pp. 2331–2333, 1999.
- [21] J. M. Bonard, N. Weiss, H. Kind, T. Stöckli, L. Forró, K. Kern, and A. Châtelain, "Tuning the field emission properties of patterned carbon nanotube films," *Adv. Mater.*, vol. 13, no. 3, pp. 184–188, 2001.
- [22] T. Y. Tsai, C. Y. Lee, N. H. Tai, and W. H. Tuan, "Transfer of patterned vertically aligned carbon nanotubes on to plastic substrates for flexible electronics and field emission devices," *Appl. Phys. Lett.*, vol. 95, no. 1, pp. 013107-1–013107-3, 2009.
- [23] X. H. Zhang, L. Gong, K. Liu, Y. Z. Cao, X. Xiao, W. M. Sun, X. J. Hu, Y. H. Gao, J. Chen, J. Zhou, and Z. L. Wang, "Tungsten oxide nanowires grown on carbon cloth as a flexible cold cathode," *Adv. Mater.*, vol. 22, no. 46, pp. 5292–5296, 2010.
- [24] I. Lahiri, V. P. Verma, and W. Choi, "An all-graphene based transparent and flexible field emission device," *Carbon*, vol. 49, no. 5, pp. 1614–1619, 2011.



Juncong She received the Ph.D. degree in physics from Sun Yat-Sen University, Guangzhou, China, in 2005.

He is a Professor of microelectronic with Sun Yat-Sen University.



Shaozeng Xu is currently pursuing the M.S. degree with the School of Physics and Engineering, Sun Yat-Sen University, Guangzhou, China.

His current research interests include modeling simulation and characterization of vacuum electronic devices.



Duo Li received the B.S. and M.S. degrees from Sun Yat-Sen University, Guangzhou, China, in 2009 and 2012, respectively.

He is currently in telephone communication industry.



Shaozhi Deng received the Ph.D. degree from Sun Yat-Sen University, Guangzhou, China.

She is a Full Professor with Sun Yat-Sen University.

www.spm.com.cn